A Nyström Discretization of a Broad-Band Augmented-Müller Surface Integral Equation

Nastaran Hendijani [1], Stephen D. Gedney [1], John C. Young [2], and Robert J. Adams [2]

[1] Department of Electrical Engineering
University of Colorado Denver, Denver, CO 80204, USA
stephen.gedney@ucdenver.edu, Nastaran.hendijani@ucdenver.edu

[2] Department of Electrical and Computer Engineering
University of Kentucky, Lexington, KY 40506, USA
john.c.young@uky.edu, robert.adams@uky.edu

Abstract — A broad-band Augmented-Müller (A-Müller) surface integral equation method for scattering from material objects is presented. The formulation incorporates surface electric and magnetic charges into the conventional Müller formulation with added constraints on the normal magnetic and electric fields. A new technique to extract the static fields is introduced which improves accuracy of computing scattered near fields at very low frequencies. The (A-Müller) formulation is discretized using the locally corrected Nyström (LCN) method. Numerical results show that the method is high-order accurate and stable over a broad frequency range from arbitrarily low to high frequencies for simply connected, multiply connected, highly lossy, high contrast and complex material geometries. The proposed formulation does not incorporate line charges, charge continuity constraints, or any frequency scaling of the degrees of freedom

Index Terms — Locally corrected Nyström method, Müller formulation, surface integral equations.

I. INTRODUCTION

An obstacle to developing accurate and stable surface integral equation formulations for scattering by perfect conducting or penetrable objects is the low frequency breakdown of the electric field integral equation $\mathcal{L}$ operator. Different strategies have been developed to address the instability including Helmholtz decomposition-based and Calderón-based stabilization methods [1, 2]. These methods have been mainly designed for use with only perfect electric conductors and may have drawbacks such as the use of global loops and increased complexity of implementation. Some methods such as the Müller formulation eliminate the low-frequency break down by transforming the hyper-singular kernel to one with a lower singularity [3]. While the Müller formulation is well conditioned, it provides inaccurate solutions at low frequencies because of catastrophic cancellation in reconstructing the fields.

Other techniques addressing the low frequency instability of the $\mathcal{L}$ operator are called augmented formulations and include surface charges as additional unknowns [4-6]. In this paper, an augmented formulation based on the conventional Müller formulation for scattering by penetrable objects is presented, wherein constraints on tangential and normal components of the fields in both the background media and the scattering media are expressed in terms of surface currents and charges and are combined in Müller form. The resulting A-Müller formulation is accurate, well-conditioned, and stable and does not include line charges, charge continuity constraints, or any frequency-dependent scaling of the unknowns

II. A-MÜLLER FORMULATION

An electromagnetic field radiated by sources in an unbounded region V_1 with material properties (μ_1, ε_1) is incident on a material object with homogeneous material properties (μ_2, ε_2) occupying a finite volume V_2 bound by the surface $S_{1,2}$. Equivalent magnetic $(\vec{M}_{1,2})$ and electric $(\vec{J}_{1,2})$ currents are introduced on $S_{1,2}$ [7]:

$$\vec{M}_{1,2} = \vec{E}_1 \times \hat{n}\big|_{S_{1,2}}, \; \vec{J}_{1,2} = \hat{n} \times \vec{H}_1\big|_{S_{1,2}}, \tag{1}$$

where $\vec{E}_1$ and $\vec{H}_1$ are the total electric and magnetic fields on $S_{1,2}$ just inside V_1, and $\hat{n}$ is the unit normal directed into V_1. The magnetic current continuity equation states:

$$\nabla \cdot \vec{M}_{1,2}(\vec{r}) = -j\omega\rho_{m_{1,2}}, \tag{2}$$

where $\rho_{m_{1,2}}$ is the magnetic surface charge density on

Submitted On: September 30, 2018
Accepted On: October 3, 2018

$S_{1,2}$ and which satisfies the boundary condition:

$$\rho_{m_{1,2}} = \hat{n}\cdot\mu_1\vec{H}_1\Big|_{S_{1,2}}. \tag{3}$$

The electric current continuity equation is defined by applying the duality theorem on (2) and (3) leading to the surface electric charge density $\rho_{e_{1,2}}$. Applying surface electric and magnetic charge continuity constraints leads to the augmented Müller formulation [3, 6]:

$$\begin{aligned}
&\mu_{r_1}\eta_0\vec{T}(\vec{r})\cdot\vec{H}_1^{inc}(\vec{r})+\mu_{r_2}\eta_0\vec{T}(\vec{r})\cdot\vec{H}_2^{inc}(\vec{r})=\\
&\frac{\mu_{r_1}+\mu_{r_2}}{2}\vec{T}(\vec{r})\cdot\tilde{\vec{J}}_{1,2}(\vec{r})\times\hat{n}\\
&-\oiint_{S_{1,2}}\vec{T}(\vec{r})\cdot\left(\mu_{r_1}\nabla G_1(\vec{r},\vec{r}')-\mu_{r_2}\nabla G_2(\vec{r},\vec{r}')\right)\times\tilde{\vec{J}}_{1,2}(\vec{r}')ds'\\
&+j\omega\eta_0\oiint_{S_{1,2}}\vec{T}(\vec{r})\cdot\vec{M}_{1,2}(\vec{r}')\left(\mu_{r_1}\varepsilon_1 G_1(\vec{r},\vec{r}')-\mu_{r_2}\varepsilon_2 G_2(\vec{r},\vec{r}')\right)ds'\\
&+\eta_0\oiint_{S_{1,2}}\vec{T}(\vec{r})\cdot\left(\nabla G_1(\vec{r},\vec{r}')-\nabla G_2(\vec{r},\vec{r}')\right)\tilde{\rho}_{m_{1,2}}(\vec{r}')ds',
\end{aligned} \tag{4}$$

where $\vec{H}_i^{inc}$ is the incident magnetic field inside V_i, and $\vec{T}(\vec{r})$ is a test vector tangential to $S_{1,2}$. $G_i(\vec{r},\vec{r}')$ is the Green's function in V_i, and $\vec{r}$ is an observation point on $S_{1,2}$. Also, $\tilde{\rho}_{m_{1,2}}=(1/\mu_o)\rho_{m_{1,2}}$, $\tilde{\rho}_{e_{1,2}}=(1/\varepsilon_o)\rho_{e_{1,2}}$, and $\tilde{\vec{J}}_{1,2}=\eta_0\vec{J}_{1,2}$ are the scaled charge and currents. μ_o, ε_o, and η_o are the free space permeability, permittivity, and characteristic impedance, respectively. Equation (4) is referred to here as the A-Müller Tangential Magnetic Field Integral Equation (TMFIE). Using (2) and (3), and combining the normal constraints on the fields in the two regions in a Müller form, the A-Müller Normal MFIE (NMFIE) can be formed:

$$\begin{aligned}
&\mu_{r_1}\eta_0\hat{n}\cdot\vec{H}_1^{inc}(\vec{r})+\mu_{r_2}\eta_0\hat{n}\cdot\vec{H}_2^{inc}(\vec{r})=\eta_0\tilde{\rho}_{m_{1,2}}(\vec{r})\\
&-\oiint_{S_{1,2}}\hat{n}(\vec{r})\cdot\left(\mu_{r_1}\nabla G_1(\vec{r},\vec{r}')-\mu_{r_2}\nabla G_2(\vec{r},\vec{r}')\right)\times\tilde{\vec{J}}_{1,2}(\vec{r}')ds'\\
&+j\omega\eta_0\oiint_{S_{1,2}}\hat{n}(\vec{r})\cdot\vec{M}_{1,2}(\vec{r}')\left(\mu_{r_1}\varepsilon_1 G_1(\vec{r},\vec{r}')-\mu_{r_2}\varepsilon_2 G_2(\vec{r},\vec{r}')\right)ds'\\
&+\eta_0\oiint_{S_{1,2}}\hat{n}(\vec{r})\cdot\left(\nabla G_1(\vec{r},\vec{r}')-\nabla G_2(\vec{r},\vec{r}')\right)\tilde{\rho}_{m_{1,2}}(\vec{r}')ds'.
\end{aligned} \tag{5}$$

Applying duality leads to the A-Müller TEFIE:

$$\begin{aligned}
&\varepsilon_{r_1}\vec{T}(\vec{r})\cdot\vec{E}_1^{inc}+\varepsilon_{r_2}\vec{T}(\vec{r})\cdot\vec{E}_2^{inc}=\frac{\varepsilon_{r_1}+\varepsilon_{r_2}}{2}\vec{T}(\vec{r})\cdot\hat{n}\times\vec{M}_{1,2}\\
&+\oiint_{S_{1,2}}\vec{T}(\vec{r})\cdot\left(\varepsilon_{r_1}\nabla G_1(\vec{r},\vec{r}')-\varepsilon_{r_2}\nabla G_2(\vec{r},\vec{r}')\right)\times\vec{M}_{1,2}(\vec{r}')ds'\\
&+j\omega/\eta_0\oiint_{S_{1,2}}\vec{T}(\vec{r})\cdot\tilde{\vec{J}}_{1,2}(\vec{r}')\left(\mu_1\varepsilon_{r_1}G_1(\vec{r},\vec{r}')-\mu_2\varepsilon_{r_2}G_2(\vec{r},\vec{r}')\right)ds'\\
&+\oiint_{S_{1,2}}\vec{T}(\vec{r})\cdot\left(\nabla G_1(\vec{r},\vec{r}')-\nabla G_2(\vec{r},\vec{r}')\right)\tilde{\rho}_{e_{1,2}}(\vec{r}')ds',
\end{aligned} \tag{6}$$

and the A-Müller NEFIE:

$$\begin{aligned}
&\varepsilon_{r_1}\hat{n}\cdot\vec{E}_1^{inc}(\vec{r})+\varepsilon_{r_2}\hat{n}\cdot\vec{E}_2^{inc}(\vec{r})=\tilde{\rho}_{e_{1,2}}(\vec{r})\\
&+\oiint_{S_{1,2}}\hat{n}(\vec{r})\cdot\left(\varepsilon_{r_1}\nabla G_1(\vec{r},\vec{r}')-\varepsilon_{r_2}\nabla G_2(\vec{r},\vec{r}')\right)\times\vec{M}_{1,2}(\vec{r}')ds'\\
&+j\omega/\eta_0\oiint_{S_{1,2}}\hat{n}(\vec{r})\cdot\tilde{\vec{J}}_{1,2}(\vec{r}')\left(\mu_1\varepsilon_{r_1}G_1(\vec{r},\vec{r}')-\mu_2\varepsilon_{r_2}G_2(\vec{r},\vec{r}')\right)ds'\\
&+\oiint_{S_{1,2}}\hat{n}(\vec{r})\cdot\left(\nabla G_1(\vec{r},\vec{r}')-\nabla G_2(\vec{r},\vec{r}')\right)\tilde{\rho}_{e_{1,2}}(\vec{r}')ds'.
\end{aligned} \tag{7}$$

Equations (4)-(7) represent A-Müller formulation. The equations are discretized using the Locally Corrected Nyström (LCN) method [3, 8-12]. The TMFIE and TEFIE in (4) and (6) are discretized using a divergence–conforming, mixed-order Nyström discretization [10, 13]. The NMFIE and NEFIE in (5) and (7) are discretized using a scalar Nyström discretization. The tangential test vectors in (4) and (6) are unitary vectors sampled at the mixed-order quadrature points [10]. The normal test vectors in (5) and (7) are sampled at scalar quadrature points.

Near interactions must be computed via local corrections [3,8-10,12]. A mixed-order Legendre polynomial basis with order $p\times(p+1)$ is used to represent the current densities [10,13], and *p*-th order polynomial complete Legendre bases are used to represent the equivalent charge densities [10]. For self-terms, the last integral on the right-hand-side of (4) and (6) and the first integral on the right-hand-side of (5) and (7) require a singularity extraction. This can be accomplished following the procedures outlined in [8-10]

III. EXTRACTING THE STATIC FIELD

As a post–processing step, it is often necessary to compute near or far scattered fields. For example, the magnetic field is calculated as

$$\begin{aligned}
\vec{H}_1^{scat}(\vec{r}) &= \oiint_{S_{1,2}}\nabla G_1(\vec{r},\vec{r}')\times\vec{J}_{1,2}(\vec{r}')ds'\\
&- j\omega\varepsilon_1\oiint_{S_{1,2}}\vec{M}_{1,2}(\vec{r}')G_1(\vec{r},\vec{r}')ds'\\
&-\frac{1}{\mu_1}\oiint_{S_{1,2}}\nabla G_1(\vec{r},\vec{r}')\rho_{m_{1,2}}(\vec{r}')ds'.
\end{aligned} \tag{8}$$

If the material object is non-magnetic, $\vec{H}_1^{scat}$ will decay in amplitude linearly as $O(\omega)$. It can be shown that the integrals involving $\vec{J}_{1,2}$ and $\rho_{m_{1,2}}$ are large valued, but their difference is very small with amplitude decaying as $O(\omega)$. This results in significant numerical errors due to finite precision.

One way to mitigate this is to extract the static solution from the dynamic solution. To this end, the A-Müller formulation in (4)-(7) can be reduced to the static solution setting $\omega=0$. For example, the static form of the TMFIE from (4) is expressed as:

$$\begin{aligned}
&\mu_{r_1}\eta_0\vec{T}(\vec{r})\cdot\vec{H}_{1_0}^{inc}+\mu_{r_2}\eta_0\vec{T}(\vec{r})\cdot\vec{H}_{2_0}^{inc}=\\
&\frac{\mu_{r_1}+\mu_{r_2}}{2}\vec{T}(\vec{r})\cdot\tilde{\vec{J}}_{1,2_0}(\vec{r})\times\hat{n}\\
&-\iint_{S_{1,2}}\vec{T}(\vec{r})\cdot\left(\mu_{r_1}\nabla G_{1_0}(\vec{r},\vec{r}')-\mu_{r_2}\nabla G_{2_0}(\vec{r},\vec{r}')\right)\times\tilde{\vec{J}}_{1,2_0}(\vec{r}')ds' \quad (9)\\
&+\eta_0\iint_{S_{1,2}}\vec{T}(\vec{r})\cdot\left(\nabla G_{1_0}(\vec{r},\vec{r}')-\nabla G_{2_0}(\vec{r},\vec{r}')\right)\tilde{\rho}_{m_{1,2_0}}(\vec{r}')ds',
\end{aligned}$$

where G_{i_0}, $i=1,2$, is the static Green function in the *i-th* medium:

$$G_{1_0}=G_{2_0}=\frac{1}{4\pi|r-r'|}=G_0, \quad (10)$$

$\vec{H}_{i_0}^{inc}$ is the static excitation magnetic field in the *i-th* medium, and $\tilde{\vec{J}}_{1,2_0}$ and $\tilde{\rho}_{m_{1,2_0}}$ are the static electric current and magnetic charge densities, respectively. The subscript 0 indicates the static solution. Similarly, the static NMFIE from (5) is expressed as:

$$\begin{aligned}
&\mu_{r_1}\eta_0\hat{n}\cdot\vec{H}_{1_0}^{inc}+\mu_{r_2}\eta_0\hat{n}\cdot\vec{H}_{2_0}^{inc}=\eta_0\tilde{\rho}_{m_{1,2_0}}(\vec{r})\\
&-\iint_{S_{1,2}}\hat{n}(\vec{r})\cdot\left(\mu_{r_1}\nabla G_{1_0}(\vec{r},\vec{r}')-\mu_{r_2}\nabla G_{2_0}(\vec{r},\vec{r}')\right)\times\tilde{\vec{J}}_{1,2_0}(\vec{r}')ds' \quad (11)\\
&+\eta_0\iint_{S_{1,2}}\hat{n}(\vec{r})\cdot\left(\nabla G_{1_0}(\vec{r},\vec{r}')-\nabla G_{2_0}(\vec{r},\vec{r}')\right)\tilde{\rho}_{m_{1,2_0}}(\vec{r}')ds'.
\end{aligned}$$

For non-magnetic materials it is assumed that $\mu_{r1}=\mu_{r2}=1$, and, (9) and (11) reduce to:

$$\eta_0\vec{T}(\vec{r})\cdot\vec{H}_{1_0}^{inc}+\eta_0\vec{T}(\vec{r})\cdot\vec{H}_{2_0}^{inc}=\vec{T}(\vec{r})\cdot\tilde{\vec{J}}_{1,2_0}(\vec{r})\times\hat{n}, \quad (12)$$

and

$$\hat{n}\cdot\vec{H}_{1_0}^{inc}+\hat{n}\cdot\vec{H}_{2_0}^{inc}=\tilde{\rho}_{m_{1,2_0}}(\vec{r}). \quad (13)$$

Thus, in the static limit, the tangential and normal magnetic fields are proportional to a superposition of the interior and exterior source fields on the boundary.

A post-processing method is proposed to improve the computation of the scattered magnetic field using a static extraction to (8) to compute the scattered magnetic field:

$$\begin{aligned}
\vec{H}_1^{scat}(\vec{r})=&\iint_{S_{1,2}}\left(\nabla G_1(\vec{r},\vec{r}')-\nabla G_0(\vec{r},\vec{r}')\right)\times\vec{J}_{1,2}(\vec{r}')ds'\\
&-\frac{1}{\mu_1}\iint_{S_{1,2}}\left(\nabla G_1(\vec{r},\vec{r}')-\nabla G_0(\vec{r},\vec{r}')\right)\rho_{m_{1,2}}(\vec{r}')ds'\\
&-j\omega\varepsilon_1\iint_{S_{1,2}}\vec{M}_{1,2}(\vec{r}')G_1(\vec{r},\vec{r}')ds' \quad (14)\\
&+\iint_{S_{1,2}}\nabla G_0(\vec{r},\vec{r}')\times\vec{J}_{1,2}(\vec{r}')ds'\\
&-\frac{1}{\mu_1}\iint_{S_{1,2}}\nabla G_0(\vec{r},\vec{r}')\rho_{m_{1,2}}(\vec{r}')ds'.
\end{aligned}$$

It is also observed for non-magnetic materials that the static current and charge densities radiate zero fields. That is:

$$\begin{aligned}
&\iint_{S_{1,2}}\nabla G_0(\vec{r},\vec{r}')\times\vec{J}_{1,2_0}(\vec{r}')ds'\\
&-\frac{1}{\mu_1}\iint_{S_{1,2}}\nabla G_0(\vec{r},\vec{r}')\rho_{m_{1,2_0}}(\vec{r}')ds'=0.
\end{aligned} \quad (15)$$

Subtracting (15) from (14) leads to the expression:

$$\begin{aligned}
\vec{H}_1^{scat}(\vec{r})=&\iint_{S_{1,2}}\left(\nabla G_1(\vec{r},\vec{r}')-\nabla G_0(\vec{r},\vec{r}')\right)\times\vec{J}_{1,2}(\vec{r}')ds'\\
&-\frac{1}{\mu_1}\iint_{S_{1,2}}\left(\nabla G_1(\vec{r},\vec{r}')-\nabla G_0(\vec{r},\vec{r}')\right)\rho_{m_{1,2}}(\vec{r}')ds'\\
&-j\omega\varepsilon_1\iint_{S_{1,2}}\vec{M}_{1,2}(\vec{r}')G_1(\vec{r},\vec{r}')ds' \quad (16)\\
&+\iint_{S_{1,2}}\nabla G_0(\vec{r},\vec{r}')\times\left(\vec{J}_{1,2}(\vec{r}')-\vec{J}_{1,2_0}(\vec{r}')\right)ds'\\
&-\frac{1}{\mu_1}\iint_{S_{1,2}}\nabla G_0(\vec{r},\vec{r}')\left(\rho_{m_{1,2}}(\vec{r}')-\rho_{m_{1,2_0}}(\vec{r}')\right)ds'.
\end{aligned}$$

This extracted formulation provides a stable numerical form for accurately computing the scattered magnetic field at low frequencies. Duality can be applied to derive a stable numerical method for computing low-frequency electric fields scattered from a magnetic material.

IV. NUMERICAL RESULTS

The proposed A-Müller formulation is evaluated by simulating scattering from a number of objects having different geometries and material properties. In all cases, the incident field is a plane wave traveling in the –*z* direction with its electric field polarized along the *x*-direction

A. PEC sphere

Initially, the electromagnetic plane-wave scattering from a one-meter radius dielectric sphere is studied. Figures 1 (a) and (b) demonstrate the root mean square (RMS) error in the scattered electric and magnetic fields calculated by the LCN discretized A-Müller formulation at 1 Hz and 50 MHz, respectively, for a surface mesh of the sphere consisting of 96 sixth-order quadrilateral cells. The errors are plotted versus LCN basis order, *p*, for different values of the relative permittivity ε_r of the dielectric material. The RMS errors are computed as:

$$\text{RMS Error}(x)=\sqrt{\frac{\sum_{i=1}^{N}\left|x^{\text{AMuller}}(\theta_i)-x^{\text{Mie}}(\theta_i)\right|^2}{\sum_{i=1}^{N}\left|x^{\text{Mie}}(\theta_i)\right|^2}}, \quad (17)$$

where $x^{\text{AMuller}}(\theta_i)$ and $x^{\text{Mie}}(\theta_i)$ refer to the scattered vector electric or magnetic fields computed by A-Müller and the analytical Mie series solution at angles $\theta_i = 0^\circ, 1^\circ, \ldots, 180^\circ$ on a semi-circle with radius 1.5 m in the $\varphi = 0^\circ$ plane. The figures demonstrate high-order convergence of the electric and magnetic fields at 1 Hz and 50 MHz for low to high contrast dielectric spheres. It is noted that the static extraction procedure has been applied to accurately calculate magnetic fields at 1 Hz.

Next, we investigate the performance of the A-Müller in comparison to the conventional Müller for scattering from a one-meter radius dielectric sphere over a wide frequency range from 1.0e-8 Hz to 1 GHz. The relative permittivity of the dielectric sphere is $\varepsilon_r = 2.0$. The surface of the sphere is discretized with 2904 fourth-order quadrilateral cells.

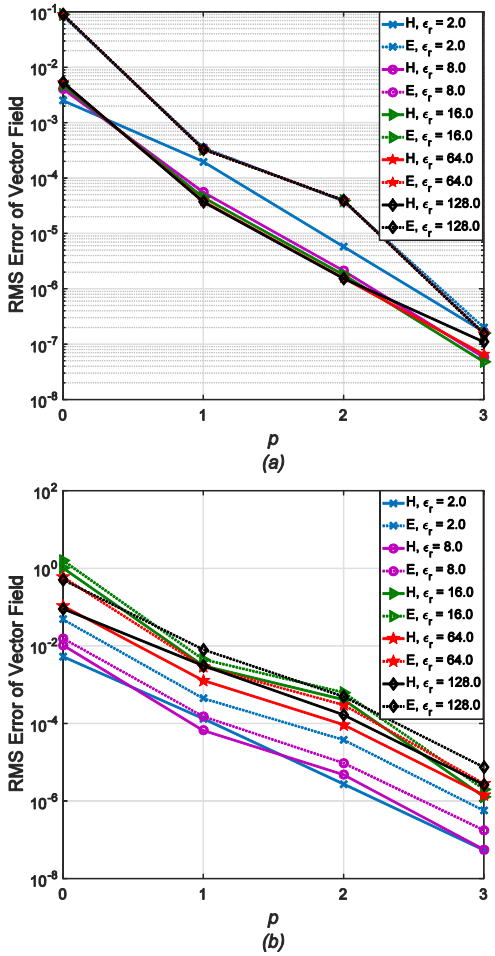

Fig. 1. RMS error in the near magnetic (H) and electric (E) fields computed via the A-Müller method, (a) at 1 Hz and (b) at 50 MHz on a semicircle with radius 1.5 m located at $\varphi = 0^\circ$.

Figures 2 (a) and (b) show the RMS error in the electric and magnetic fields scattered by the dielectric sphere. The fields area computed on a semicircle with radius 1.5 m located at $\varphi = 0^\circ$ using both the A-Müller formulation with and without the static extraction and the Müller formulation for LCN basis orders $p = 0$ and p=1. The data exhibits high errors in the Müller formulation at low frequencies due to catastrophic cancellation in reconstructing the electric and magnetic fields. The A-Müller with static extraction has excellent accuracy over a wide frequency range starting from arbitrarily low frequencies. The errors from Müller and A-Müller start to grow at a threshold frequency around 200 MHz where the number of samples per wavelength is 10.

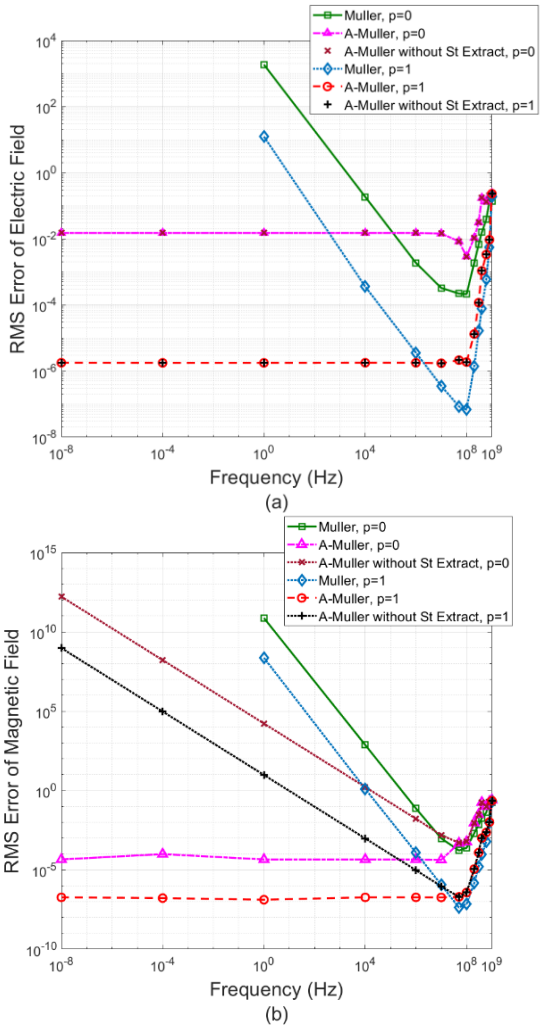

Fig. 2. The RMS error in vector, (a) electric field and (b) magnetic field scattered from a dielectric sphere computed by A-Müller without and with the static extraction (St Extract) and Müller formulations on a semicircle with radius 1.5 m located at $\varphi = 0^\circ$.

Figure 3 plots the condition number of A-Müller and Müller system matrices versus frequency for scattering from the dielectric sphere. The system matrices were pre-conditioned with a left/right iterative diagonal matrix scaling algorithm [14] to eliminate row magnitude disparity. The A-Müller condition number starts oscillating after 400 MHz.

Unlike the Müller and PMCHWT, the VIE provides accurate solutions for exterior scattered electric and magnetic fields at low frequencies. However, one limitation of the VIE is that the condition number of the system matrix at low frequencies grows linearly with increasing material contrast. Figure 4 displays the condition number of the A-Müller and VIE system matrices versus relative permittivity, ε_r, for scattering from a one-meter radius sphere at 1 Hz. The surface of the sphere is meshed with 96 sixth order quadrilateral cells. The LCN basis order is $p=0$. The figure shows that the condition number of the VIE is increasing linearly with material contrast; however, the condition number of the A-Müller formulation is nearly constant as the relative permittivity increases.

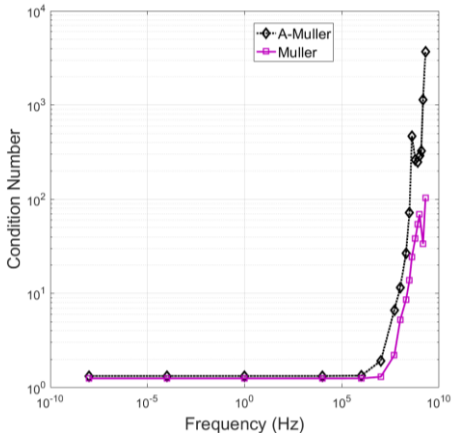

Fig. 3. Condition number of the iteratively scaled A-Müller and Müller system matrices for scattering from the dielectric sphere versus frequency.

B. Dielectric tori

To evaluate the performance of the A-Müller formulation for multiply connected geometries, a nested torus structure consisting of two dielectric tori was simulated. The two torus structure has a z-axis of revolution. The larger torus has a major radius of 1 m and a minor radius of 0.5 m, respectively. The smaller torus has a major radius of 1 mm and a minor radius of 0.5 mm, respectively. The larger and smaller tori surfaces are meshed with quadrilateral cells having average edge lengths, respectively, of 0.2 m and of 0.2 mm for a total of 384 quadratic quadrilateral cells. The dielectric tori both have a relative permittivity $\varepsilon_r = 8.0$. The LCN basis order is $p=1$.

Figure 5 demonstrates the radar cross section (RCS) of the two torus structure at 300 MHz computed using A-Müller, Müller, and PMCHWT formulations. The three solutions show excellent agreement. Figures 6 (a) and (b) display the magnitude of the scattered electric and magnetic fields at 1 Hz calculated using A-Müller, Müller, and PMCHWT formulations and using a volume integral equations (VIE) for scattering from the two torus structure. The volume mesh used for the VIE consists of 576 hexahedral cells with an average edge length the same as the applied surface mesh. Very good agreement is observed between the A-Müller and the VIE results. Moreover, the data confirm the low frequency break-down of the PMCHWT and Müller formulations in reconstructing of the fields at low frequencies.

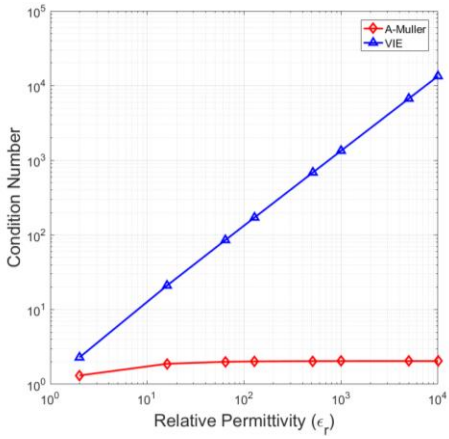

Fig. 4. Condition number of the iteratively scaled A-Müller and VIE system matrices versus relative permittivity, for scattering from a one-meter radius dielectric sphere at 1Hz.

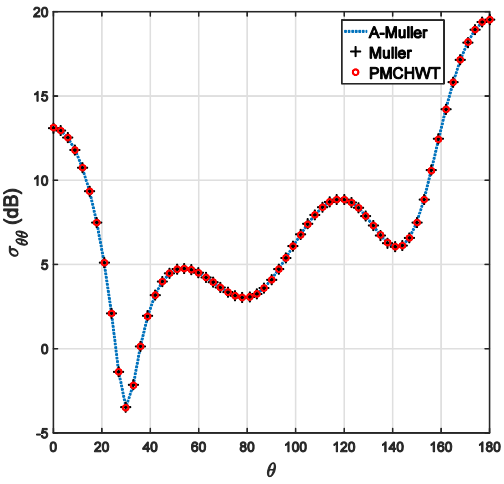

Fig. 5. RCS at 300 MHz for plane wave scattering from the two torus structure.

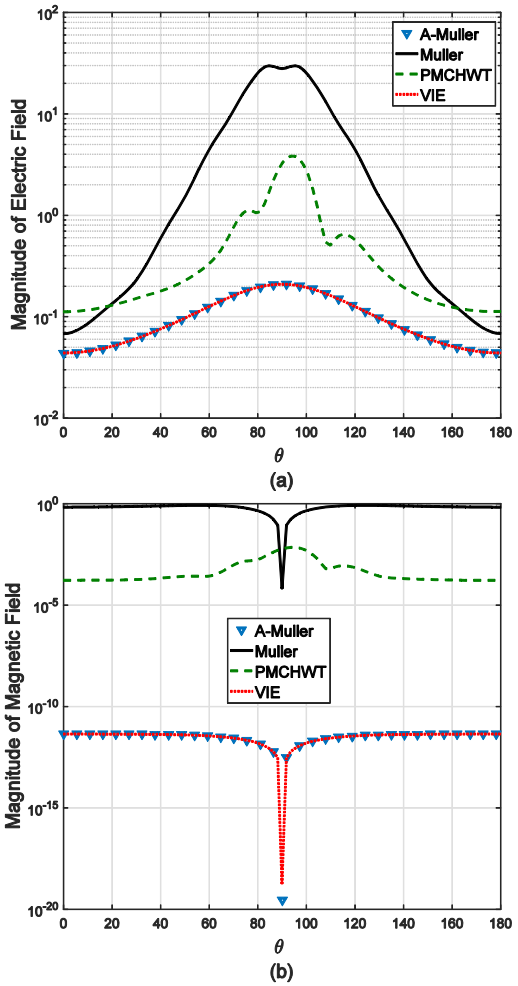

Fig. 6. Scattered (a) electric field and (b) magnetic field at 1 Hz for the two torus structure on a semi-circle with radius 1.5 m at $\varphi = 0^\circ$.

Figures 7 (a) and (b) illustrate the singular values of the A-Müller, Müller, PMCHWT, and VIE system matrices for the two torus configuration at 300 MHz and 1 Hz, respectively. The system matrices are preconditioned using an iterative scaling algorithm [14]. The figures indicate that A-Müller provides a well-conditioned system matrix for multiply connected geometries at both low and high frequencies.

C. Spherical shell of steel

The A-Müller formulation is also compared to a quasi-magnetostatic volume integral equation (VIE) [15] method by simulating the scattering from conducting materials at low frequencies. A spherical shell of steel characterized by electric conductivity $\sigma = 1.37e+6$ S/m and relative permeability $\mu_r = 68.0$. The shell has an inner radius of 1 cm and outer radius of 3 cm. The mesh cells have an average edge length of 0.35 cm leading to 1160 quadrilateral cells for the A-Müller formulation and 716 hexahedral cells for the VIE.

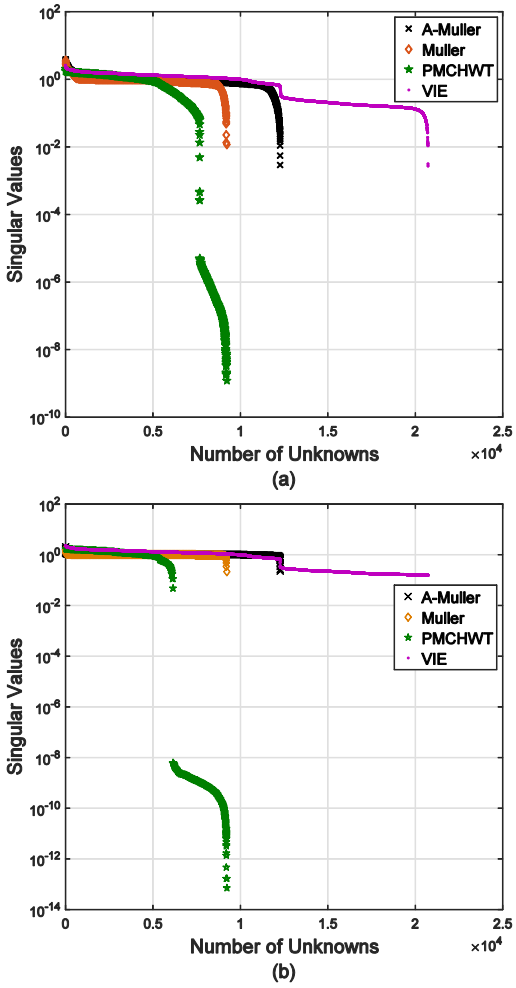

Fig. 7. Singular values of the A-Müller, Müller, PMCHWT, and VIE system matrices for the two torus case at: (a) 300 MHz and at (b) 1Hz.

Figure 8 displays the magnitude of real and imaginary parts of the azimuthal component of the magnetic field (H_φ) scattered from the steel shell computed using the A-Müller formulation and a quasi-magnetostatic VIE at 10 Hz on a semicircle with radius 3.5 cm at $\varphi = 0^\circ$ plane.

The radial and polar (r and θ) components of the magnetic field are not shown since their magnitudes are negligible. Good agreement is observed between the results from the A-Müller formulation and from the quasi-magnetostatic VIE.

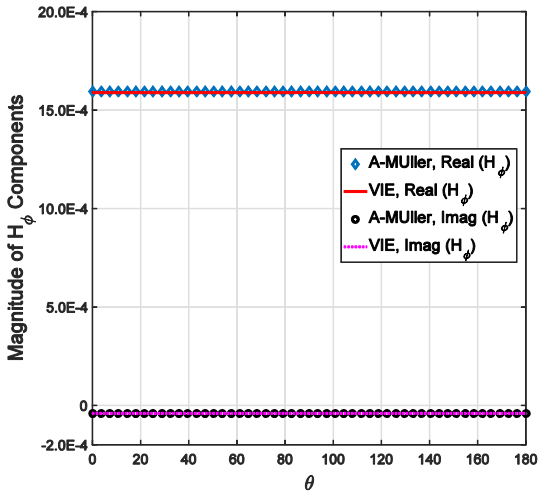

Fig. 8. Magnitude of real and imaginary parts of the azimuthal component of magnetic field scattered from the steel shell computed on a semicircle with radius 3.5 cm at $\varphi = 0^\circ$ plane.

VI. CONCLUSION

In this paper, the LCN discretization of an Augmented-Müller surface integral equation for scattering from material objects was presented. The formulation incorporated surface electric and magnetic charges into the conventional Müller formulation with constraints on the normal magnetic and electric fields on material boundaries. To improve the accuracy of the computation of low-frequency magnetic fields scattered by lossy dielectric structures, a novel static extraction method was introduced. The extraction is applied strictly as a post-processing operation and does not alter the system matrix in any way. Numerical results provided validate that the method is high-order accurate and stable over a broad frequency range from arbitrarily low to high frequencies for simply and multiply connected, lossy, high contrast materials.

ACKNOWLEDGMENT

This work was supported in part by Office of Naval Research Grants N00014-16-1-2941.

REFERENCES

[1] F. P. Andriulli, K. Cools, H. Bagci, F. Olyslager, A. Buffa, S. Christiansen, *et al.*, "A multiplicative Calderon preconditioner for the electric field integral equation," *IEEE Transactions on Antennas and Propagation*, vol. 56, pp. 2398-2412, Aug. 2008.

[2] G. Vecchi, "Loop-star decomposition of basis functions in the discretization of the EFIE," *IEEE Transactions on Antennas and Propagation*, vol. 47, pp. 339-346, Feb. 1999.

[3] A. M. Zhu, S. D. Gedney, and J. L. Visher, "A study of combined field formulations for material scattering for a locally corrected Nystrom discretization," *IEEE Transactions on Antennas and Propagation*, vol. 53, pp. 4111-4120, Dec. 2005.

[4] M. Taskinen and P. Yla-Oijala, "Current and charge integral equation formulation," *IEEE Transactions on Antennas and Propagation*, vol. 54, pp. 58-67, Jan. 2006.

[5] T. Xia, H. Gan, M. Wei, W. C. Chew, H. Braunisch, Z. G. Qian, *et al.*, "An integral equation modeling of lossy conductors with the enhanced augmented electric field integral equation," *IEEE Transactions on Antennas and Propagation*, vol. 65, pp. 4181-4190, Aug. 2017.

[6] P. Yla-Oijala and M. Taskinen, "Well-conditioned Muller formulation for electromagnetic scattering by dielectric objects," *IEEE Transactions on Antennas and Propagation*, vol. 53, pp. 3316-3323, Oct. 2005.

[7] R. F. Harrington, "Boundary integral formulations for homogeneous material bodies," *Journal of Electromagnetic Waves and Applications*, vol. 3, pp. 1-15, 1989.

[8] L. F. Canino, J. J. Ottusch, M. A. Stalzer, J. L. Visher, and S. M. Wandzura, "Numerical solution of the Helmholtz equation in 2D and 3D using a high-order Nyström discretization," *Journal of Computational Physics*, vol. 146, pp. 627-663, 1998.

[9] S. D. Gedney, "On deriving a locally corrected Nyström scheme from a quadrature sampled moment method," *IEEE Transactions on Antennas and Propagation*, vol. 51, pp. 2402-2412, Sep. 2003.

[10] S. D. Gedney and J. C. Young, "The locally corrected Nyström method for electromagnetics," in *Computational Electromagnetics: Recent Advances and Engineering Applications*, R. Mittra, Ed., ed New York: Springer, 2013, pp. 149-198.

[11] M. Shafieipour, I. Jeffrey, J. Aronsson, and V. I. Okhmatovski, "On the equivalence of RWG method of moments and the locally corrected Nystrom method for solving the electric field integral equation," *IEEE Transactions on Antennas and Propagation*, vol. 62, pp. 772-782, Feb. 2014.

[12] F. Vico, M. Ferrando-Bataller, A. Valero-Nogueira, and A. Berenguer, "A high-order locally corrected Nystrom scheme for charge-current integral equations," *IEEE Transactions on Antennas and Propagation*, vol. 63, pp. 1678-1685, Apr. 2015.

[13] S. D. Gedney, A. Zhu, and C. C. Lu, "Study of mixed-order basis functions for the locally-corrected Nyström method," *IEEE Transactions on Antennas and Propagation*, vol. 52, pp. 2996-3004,

Nov. 2004.
[14] J. Cheng, R. J. Adams, J. C. Young, and M. A. Khayat, "Augmented EFIE with normally constrained magnetic field and static charge extraction," *IEEE Transactions on Antennas and Propagation*, vol. 63, pp. 4952-4963, Nov. 2015.
[15] J. C. Young and S. D. Gedney, "A locally corrected Nyström formulation for the magnetostatic volume integral equation," *IEEE Transactions on Magnetics*, vol. 47, pp. 2163-2170, Sep. 2011.

Nastaran Hendijani received the B.S. degree in Electrical Engineering from Amirkabir University of Technology (Tehran Polytechnic), Tehran, Iran, in 2003, and the M.S. degree in Electrical Engineering from Iran University of Science and Technology (IUST), Tehran, Iran, in 2006 and the Ph.D. degree in Electrical and Computer Engineering from University of Kentucky, Lexington, KY, in 2015.

From 2009 to 2012, she was a Research Assistant in the Department of Electrical and Computer Engineering at Virginia Polytechnic Institute and State University (Virginia Tech). From 2012 to 2015, she was a Research Assistant in the Department of Electrical and Computer Engineering at the University of Kentucky. Since 2015 she has been a Post-doctoral Researcher in the Department of Electrical and Computer Engineering at the University of Colorado, Denver, CO. Her research interests are in applied and computational electromagnetics, high-performance computing, and radio frequency identification.

Stephen D. Gedney received the B.Eng.-Honors degree from McGill University, in 1985, and the M.S. and Ph.D. degrees in Electrical Engineering from the University of Illinois, Urbana-Champaign, IL, in 1987 and 1991, respectively.

He is currently the Chair and the Don and Karen White Professor of the Electrical Engineering Department at the University of Colorado Denver (UCD). Previously he was a Professor of Electrical Engineering at the University of Kentucky from 1991–2014. He worked for the U.S. Army Corps of Engineers, Champaign, IL ('85-'87). He was a Visiting Professor at the Jet Propulsion Laboratory, (92',93'), HRL Laboratories ('96-'97) and Alpha Omega Electromagnetics ('04-'05). He received the Tau Beta Pi Outstanding Teacher Award in 1995 and 2013. He is a Fellow of the IEEE and Member of Tau Beta Pi.

John C. Young received the B.E.E. degree in Electrical Engineering from Auburn University in 1997, the M.S. degree in Electrical Engineering from Clemson University in 2000, and the Ph.D. degree in Electrical Engineering also from Clemson University in 2002. He received a National Science Foundation Graduate Fellowship in 1998 and served as a Graduate Research Assistant at Clemson University from 1997 to 2002. He is currently an Assistant Professor in the Department of Electrical and Computer Engineering at the University of Kentucky, Lexington, KY. He is a Senior Member of IEEE and a Member of URSI Commission B, Tau Beta Pi, and Eta Kappa Nu.

Robert J. Adams received the B.S. degree from Michigan Technological University, Houghton, MI, USA, in 1993, and the M.S. and Ph.D. degrees in Electrical Engineering from Virginia Tech, Blacksburg, VA, USA, in 1995 and 1998, respectively. From 1999 to 2000, he was a Research Assistant Professor with Virginia Tech. He is currently a Professor with the Department of Electrical and Computer Engineering, University of Kentucky, Lexington, KY, USA. His current research interests include applied and computational electromagnetics.